A Novel Explicit Disturbance Model-based Robust Damping of Inter-Area Oscillations through MTDC Grids Embedded in AC Systems

Abhishek Banerjee, *Student Member, IEEE*, Nilanjan Ray Chaudhuri, *Senior Member, IEEE*, and Rajesh Kavasseri, *Senior Member, IEEE*

***Abstract*—This paper presents a novel approach to damp inter-area oscillations by designing a robust multi-input multi-output (MIMO) supplementary controller for Multiterminal DC (MTDC) systems embedded in AC grids. The key idea to achieve robustness lies in explicitly modeling the MTDC current injection as disturbances using an $\mathcal{H}_\infty$ mixed-sensitivity formulation in the Linear Matrix Inequality (LMI) framework. Control directions are established by selecting wide-area feedback signals and the Relative Gain Array computation. Robustness is assessed through dynamic simulations for scenarios including: (a) disturbances on the AC side, (b) disturbances on the DC-side such as loss of a converter pole including actuator, (c) partial loss of feedback signal, and (d) communication latencies. The performance of the proposed controller is compared against the conventional $\mathcal{H}_\infty$ based design, using a 4-terminal DC grid embedded within the New England-New York test system. The results suggest that the proposed approach demonstrates superior performance following DC-side disturbances, actuator outages, and latency.**

***Index Terms*—Linear Matrix Inequality (LMI), Mixed-Sensitivity, Explicit Disturbance Modeling, Inter-area Oscillations, Multiterminal DC (MTDC), Robustness, $\mathcal{H}_\infty$**

NOMENCLATURE

Converter Stations

$I_{gX}^{p/n}$	X-axis current component of positive/negative poles in each converter station
$I_{gY}^{p/n}$	Y-axis current component of positive/negative poles in each converter station
I_{pcc}	Current injections at the point of common coupling
$P_{pcc}^{p/n}$	Power output of positive/negative pole of converter stations
$V_{dc}^{p/n}$	DC voltage of positive/negative pole converter stations

Control Design

d	Disturbance input
F_l	Lower fractional transformation
G_d	Disturbance plant
G_u	Nominal plant
N	Closed loop transfer function from $[\frac{r}{d}]$ to $[\frac{z_1}{z_2}]$
P	Generalized plant
w	Exogenous inputs
W_1S	Weighted sensitivity
W_2KS	Weighted control sensitivity
y	Combined output of G_d and G_u
y_p	Output feedback signals
z	Regulated outputs

A. Banerjee and R. Kavasseri are with Department of Electrical & Computer Engineering, North Dakota State University, Fargo, ND, USA (e-mail: *abhishek.banerjee@ndsu.edu, rajesh.kavasseri@ndsu.edu*).

N.R. Chaudhuri is with Department of Electrical Engineering & Computer Science, Pennsylvania State University, State College, PA, USA (e-mail: *nuc88@engr.psu.edu*). This work was supported by NSF under grant 1656983.

I. INTRODUCTION

VOLTAGE Source Converter (VSC)-based Multiterminal DC (MTDC) grids are beginning to show significant promise in integrating offshore wind resources to onshore grids - thus attracting recent research attention towards modeling [1], [2] and control [3], [4] of such systems. In general point-to-point HVDC schemes suffer from certain issues, which can be overcome by an MTDC grid. As a result, such systems can also be beneficial for onshore installations. The advantages of MTDC grids include: (a) Improved reliability in face of a single-point failure, (b) Reduced capacity and reserve capacity requirement since the peak demand of different AC systems do not occur at the same time, (c) Reduced curtailment from wind farms, (d) reduced variability in renewable generation, ease of annual and preventive maintenance of the generators and the converter systems and energy trading between multiple regions like today's AC power systems, and (e) Lower energy cost. For further explanation on points (a) (d), please refer to [11], and for point (e), please see [9], [10].

The operators of these MTDC grids connected to AC systems with multiple areas will face the typical challenges of stabilizing poorly-damped inter-area oscillations. The idea that VSC MTDC converters can provide damping support to the surrounding AC system by virtue of their ability for fast modulation of active power injections has been explored in recent literature [5]–[8], [11], [12] to design supplementary controllers. In this emerging area, it is important as pointed out in [6] to understand how the choice of controller structure influences improvements to dynamic system performance. Thus motivated, our goal is to design a supplementary controller, which can damp multiple modes and remain robust even after DC-side contingencies including actuator outages occur. The novelty lies in explicitly incorporating the MTDC current injection as disturbances in the control design using an $\mathcal{H}_\infty$ mixed-sensitivity formulation in the Linear Matrix Inequality (LMI) framework. This allows the control performance to be robust even when there are failures on the DC side, an aspect overlooked in recent literature. We summarize our salient contributions while drawing distinctions from prior related work as follows:

Unlike [6]–[8], [11], [12], we incorporate robustness against

DC grid disturbances into the design formulation itself and demonstrate control performance in the wake of DC-side contingencies including converter outages. To that end, the design problem presented here includes disturbance rejection into control design by introducing a novel explicitly modeled disturbance plant as opposed to the conventional way of modeling disturbances in the LMI problem in the $\mathcal{H}_\infty$ framework, as in our prior work in [12]. This has not been reported in any prior work on MTDC systems. Moreover, we have taken into account a true MIMO design by considering two converter stations in the control design formulation to damp the targeted inter-area modes, as opposed to using only two poles of a single converter station as in [12]. This presents a tough challenge in determining the control directions in an MTDC system due to increased interactions, which has been established by RGA computations. Furthermore, robustness has been assessed on several major outages, feedback signal loss, and communication latencies. A comparison has been done with the prevailing standard $\mathcal{H}_\infty$ design for power oscillation damping to demonstrate the benefits of the proposed design over an existing technique.

Unlike [7], [8] where a single mode of interest is considered, we show that the proposed method can target multiple poorly damped modes of interest and improve their damping significantly without compromising other non-targeted modes. Unlike [11] where essentially point-to-point DC links are considered to test the control strategy, we demonstrate control performance on truly MTDC grids embedded in the AC system.

We emphasize that the MTDC system or its placement is not considered solely for the purpose of damping improvement for AC systems. Neither do we consider $\mathcal{H}_\infty$-based design blindly as a "black-box" tool for robustness. Instead, our key contributions lie in modifying the design approach itself by explicitly modeling disturbances, which allows the problem to be cast in terms of an $\mathcal{H}_\infty$ optimization. This renders our approach generic and applicable to hybrid systems regardless of the size or placement of the MTDC system within the AC system.

The paper is organized with modeling aspects described in Sec. II, control formulation and solution in Sec. III, system description and signal selection in Sec. IV, simulation results in Sec. V, and conclusions in Sec.VI.

II. Modeling and Control of MTDC Grid

We consider a bipolar VSC-MTDC grid with a metallic return network. Converters are represented by their averaged models and transmission lines between converter stations are represented by π-section models. Figure 1 shows the i^{th} converter station with positive (p) and negative poles (n). Further details can be found in [2], [13].

A. Inner and Outer Control Loops

As shown in Fig. 2, the converter stations are assumed to operate under active power-common DC link voltage droop control where the error in the square of a *common* DC voltage V_{dc_comm} is drooped against the power error. Here, the DC link voltage from a common converter station is communicated

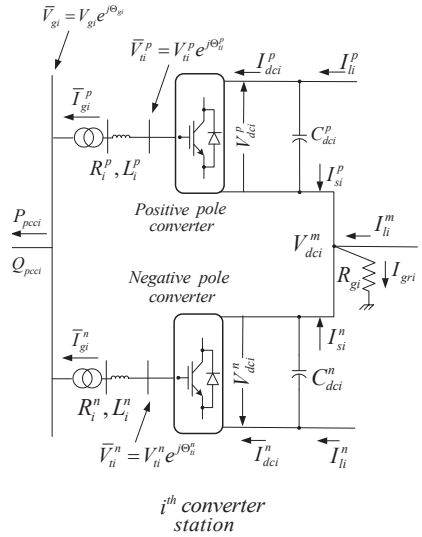

Fig. 1. The i^{th} converter station of the MTDC grid.

to the other stations [3]. The real power reference P_{pcck}^{p*} is modulated using control input P_{mod}^{p} for power oscillation damping.

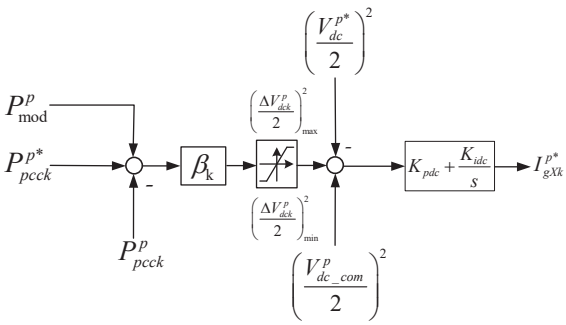

Fig. 2. Active power-DC link voltage droop control for the positive pole of the k^{th} converter station. The real power reference P_{pcck}^{p*} is modulated using control input P_{mod}^{p} for power oscillation damping. Identical control is used for the negative pole.

As shown in Fig. 3 the converter stations are modeled and controlled using well-known decoupled vector control strategy in the $d-q$ frame. We denote this frame as the $X-Y$ frame to avoid conflict with the $d-q$ frame notations commonly used for individual generator models [2], [13]. The PI controller shown in Fig. 2 derives the X-axis current reference I_{gX}^{p*} for the inner current control loop of the positive pole converter. An identical control scheme is used for the negative pole.

B. Integration with Surrounding AC System

The differential-algebraic equation model of the multi-machine AC system is built on a current injection framework. Similarly, the MTDC portion is also modeled using this current injection framework. Interface of the converter and controller models along with the DC network model is well understood and not presented here. Interested readers are refered to [13] for details.

III. Control Formulation and Design

A. Explicit Modeling of Disturbance Rejection

Our key contribution is in framing a robust control problem where DC-side contingencies in the MTDC grid can be

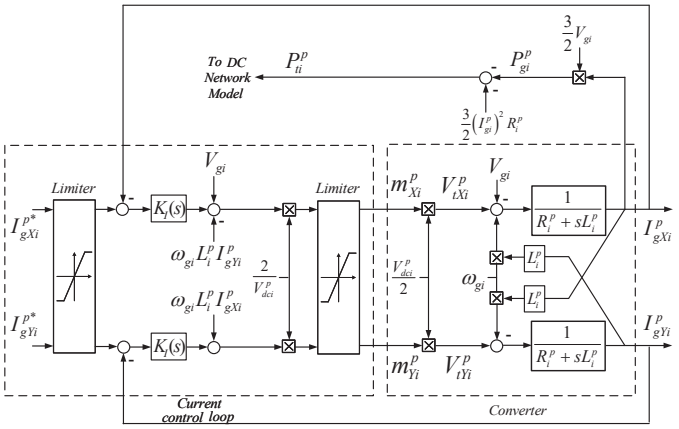

Fig. 3. Model of the positive pole converter of the i^{th} converter station with its inner current control loop.

incorporated as a disturbance in a LMI formulation. Since the MTDC portion is modeled on a current injection framework, any disturbance on the DC side will induce corresponding changes in the current injections into the AC grid. In turn, this will perturb the currents I_{gX} and I_{gY} in the inner current control loop of converter station poles, which have been modeled in the $X_i - Y_i$ reference frame (see Fig. 3). Since our model consists of positive and negative poles in each converter station, this perturbed current can be resolved into four such current components $I_{gX}^{p/n}$, $I_{gY}^{p/n}$ for both poles of a converter station, Fig 4. These current components can be further combined into the current injections at the positive and the negative poles $I_g^{p/n}$ of the converters, see Fig 4.

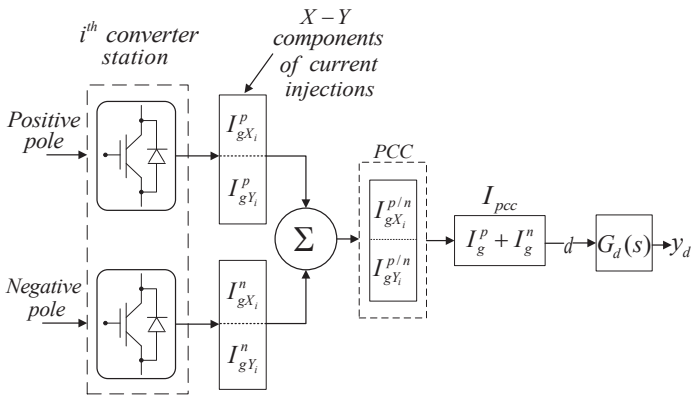

Fig. 4. DC-side contingencies modeled as a disturbance plant $G_d(s)$ using current injections I_{pcc} as input and feedback signals y_d used for damping control as output.

Therefore, the current I_{pcc} at the point of common coupling (PCC) comprising the current injections of the positive and negative poles is modeled as the disturbance input d to the MTDC grid. Figure 4 represents the complete modeling of the disturbance plant $G_d(s)$ where in a nutshell, the input are the injected currents from the positive and negative poles of the i^{th} converter station and the output are the feedback signals y_d used for damping control. Note that the synthesized disturbance plant $G_d(s)$ has the same poles as in the plant $G_u(s)$, which represents the MIMO linear model of the system between control input u denoted by P_{mod} signals shown in Fig. 2 and the feedback signals denoted as y_p used for damping control. The Mixed-Sensitivity formulation involving plants $G_d(s)$ and $G_u(s)$ is described next.

B. Mixed Sensitivity Formulation

With the explicitly modeled disturbances, we translate the Stacked Sensitivity problem to an $\mathcal{H}_\infty$ optimization.

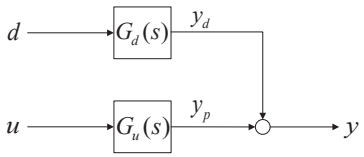

Fig. 5. Combined output of the nominal and the disturbance plant.

The modeled disturbance plant $G_d(s)$ is incorporated into the formulation of the generalized plant P and further included in the LMI by formation of the partitioned plant. The combined output as shown in Fig. 5 can be expressed as $y = G_d(s)d + G_u(s)u$ where,

$$G_d = C(sI - A)^{-1}B_d,\ G_u = C(sI - A)^{-1}B_u \tag{1}$$

The proposed control scheme is depicted in Fig. 6 where d, r are the exogenous input including disturbances. The regulated output are z_1 and z_2, and being a regulator problem, the reference $r = 0$.

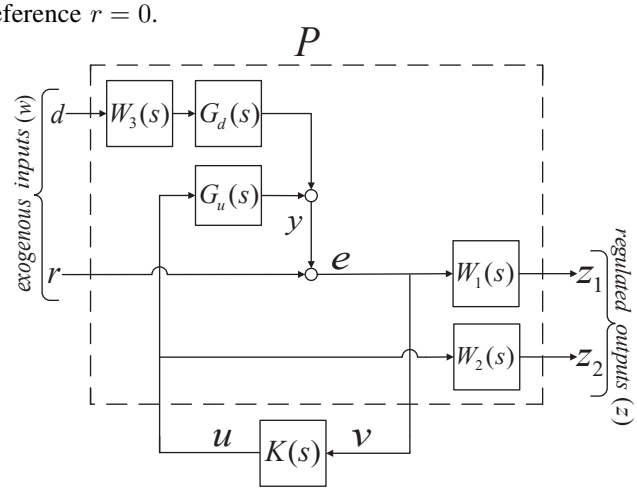

Fig. 6. Mixed sensitivity with explicit disturbance rejection

The generalized plant P, including the weighting filters and the disturbance plant can be partitioned as,

$$P = \left[\begin{array}{c|c} P_{11} & P_{12} \\ \hline P_{21} & P_{22} \end{array}\right] \tag{2}$$

such that its parts resemble with z, v, w, and u and in the generalized control configuration as,

$$\begin{aligned} z &= P_{11}w + P_{12}u \\ v &= P_{21}w + P_{22}u \end{aligned} \tag{3}$$

Expanding this to the proposed mixed-sensitivity scheme as shown in Fig. 6, the generalized plant P is obtained as,

$$P = \left[\begin{array}{c|c} W_1W_3G_d & W_1G_u \\ 0 & W_2 \\ \hline G_d & G_u \end{array}\right] \tag{4}$$

After the interconnecting structure has been used to determine P, the next step is to synthesize a sub-optimal controller, and combine the controller in the structure in Fig. 6, to obtain the closed-loop form N, which represents the closed-loop

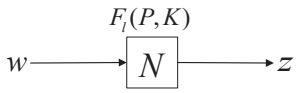

Fig. 7. General block diagram for analysis of closed-loop performance.

transfer function, see Fig. 7, from the exogenous input to the regulated output, i.e, from $[\frac{r}{d}]$ to $[\frac{z_1}{z_2}]$. N is calculated using a Lower Fractional Transformation (LFT), [15] which yields,

$$N = P_{11} + P_{12}K\left(I - P_{22}K\right)^{-1}P_{21} \cong F_l\left(P, K\right) \quad (5)$$

The $\mathcal{H}_\infty$ optimization problem now boils down to find a stabilizing controller K to minimize the cost function,

$$\left\| \begin{bmatrix} W_1S & W_1SG_dW_3 \\ W_2KS & W_2KSG_dW_3 \end{bmatrix} \right\|_\infty \quad (6)$$

which is the $\mathcal{H}_\infty$ norm of the transfer function from $[\frac{r}{d}]$ to z. Since in our case $r = 0$, the cost function in (6) simplifies to (7). The goal of the $\mathcal{H}_\infty$ design is minimizing (7) for guaranteed robustness.

$$\left\| \begin{bmatrix} W_1SG_dW_3 \\ W_2KSG_dW_3 \end{bmatrix} \right\|_\infty \quad (7)$$

This $\mathcal{H}_\infty$ optimization problem in (7) involves solutions of LMI's for minimizing $\|N\|_\infty$, which guarantees asymptotic stability. This is a well studied aspect and it involves the solutions of LMI's in regard to the bounded real lemma [16], [17], using Schur's formula for the determinant of a partitioned matrix [15], and is not discussed here. This LMI problem can be solved by using the Robust Control Toolbox in Matlab [22]. An additional constraint to place all poles on the left-half of of the s-plane within a conic sector was considered to ensure the desired closed-loop damping ratio [18], [19], [20].

IV. Test System and Damping Controller Synthesis

A. Test System

The MTDC grid consists of four converter terminals, which are interconnected to the 16-machine NETS-NYPS system [14] as shown in Fig. 8. The nominal real and reactive powers at the PCC of the converter stations are annotated in this figure. All generators are represented by subtransient models and eight of them ($G1 - G8$) are equipped with the IEEE DC1A excitation system. The rest of the machines are under manual excitation control, and $G9$ is equipped with a static exciter and a power system stabilizer (PSS). Constant impedance type loads are considered. The dynamic data and base case conditions are as in [14].

B. Signal Selection Criterion

Eigenvalue analysis reveals that the system has two poorly damped inter-area modes of interest: (0.2 Hz at 1.5 %) and (0.47 Hz at 3.3 %), which are shown in Table I. Since the specific objective of the damping controller is to improve the damping of these two modes without negatively impacting the others, it is necessary to learn the interaction among input and output, and identify the most appropriate control directions.

TABLE I
Damping ratios, frequencies and settling times of the inter-area modes in Test System with Proposed Control

Design Criterion, $\zeta_{min} = 6.5\%$						
Mode no.	OPEN-LOOP			CLOSED-LOOP		
	ζ	f, Hz	T, s	ζ	f, Hz	T, s
1.	**0.015**	0.201	204.20	**0.285**	0.238	8.99
2.	**0.033**	0.475	40.25	**0.091**	0.473	14.68
3.	0.081	0.537	14.64	0.085	0.528	14.12
4.	0.053	0.792	15.25	0.054	0.792	14.89

To that end, residue analysis was performed for appropriate selection of feedback signals and control input. In MIMO systems, the angle of the residue is important as well. The phase compensation required at each modal frequency is closely related to the phase angles of the residue [21]. The residue analysis of the linear model shown in Table II reveals that the best selection of feedback signals are P_{27-53} across mode 1 and P_{13-17} across mode 2 whereas converter stations $\#1$ and $\#3$ are the best choice for the control input.

Relative Gain Array (RGA): In a true MIMO sense, RGA is used to corroborate the input/output pairing choices obtained from the signal selection. The RGA of a non-singular square matrix G is a square matrix defined as

$$RGA\left(G\right) = \Lambda\left(G\right) \cong G \times \left(G^{-1}\right)^T \quad (8)$$

where $\times$ denotes element-by-element multiplication (the Schur or Hadamard product). RGA can also be computed for non-square matrices by the method of pseudoinverse [15].

RGA values are useful to guide the selections because: (a) values close to 1 show favourable pairing [24] for centralized control scheme and (b) negative entries indicate too much interaction and not suitable for pairing. In our design, RGA was calculated for the nominal plant $G_u(s)$ with results shown in Table III, where the input are the columns and the feedback signals are the rows. The analysis clearly affirms with the input/output pairing choices made earlier by residue calculations.

As seen in Table III, for the feedback signal P_{13-17}, converter station #3 shows the best possibility of pairing with RGA value being closest to unity. Although converter station #4 negative pole has a closer value than #3 negative pole, we choose #3 as the best possible case because it has a higher modal controllability index for mode 2. For feedback signal P_{27-53}, converter #1 stands closest to unity which validates

TABLE II
Residues showing normalized magnitudes and angle

Feedback	Input Signals				
	Converter #1		Converter #3		Mode 1
	mag	ang (degree)	mag	ang (degree)	
$P_{(27-53)}$	1	-158.88	1	33.02	
$P_{(13-17)}$	0.1325	39.71	0.1325	-128.37	

Feedback	Input Signals				
	Converter #1		Converter #3		Mode 2
	mag	ang (degree)	mag	ang (degree)	
$P_{(27-53)}$	0.0632	-57.97	0.0632	-11.04	
$P_{(13-17)}$	1	125.03	1	171.96	

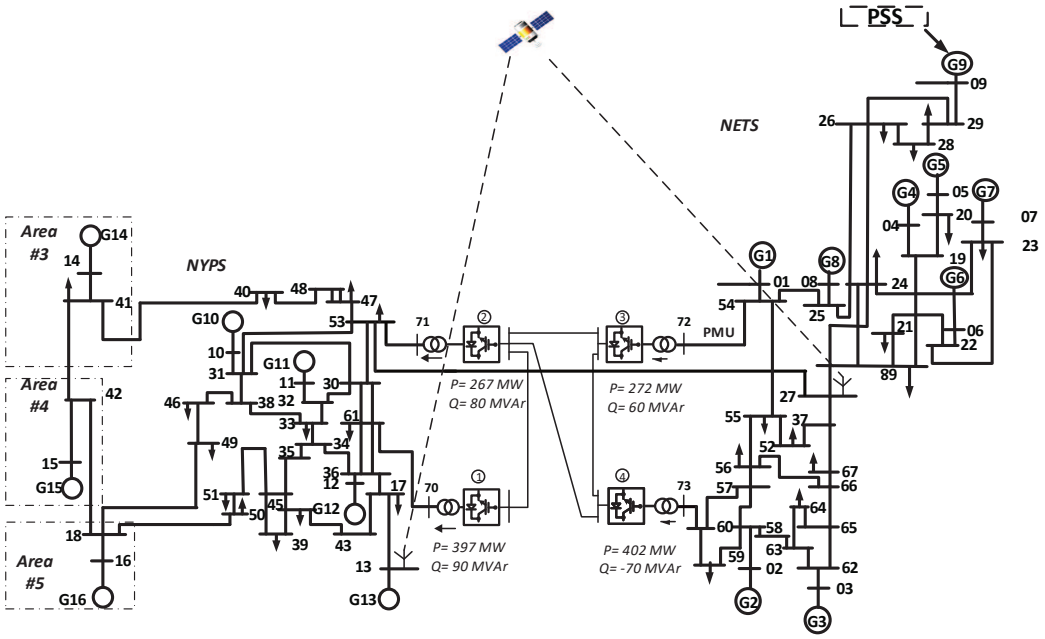

Fig. 8. Bipolar MTDC grid with metallic return (single line diagram) connected to 16-machine AC system.

TABLE III
RELATIVE GAIN ARRAY

Output	Input			
	Converter #1	Converter #2	Converter #3	Converter #4
$P_{(13-17)}$	-0.311	-0.121	0.655	0.533
$P_{(27-53)}$	0.793	0.311	-0.249	-0.172

our signal selection.

C. Process for Damping Controller Synthesis

1) Damping Criterion: The closed loop poles of the critical modes are placed within a conic sector with inner angle θ and the apex at the origin [19], [20] to ensure a minimum damping ratio $\zeta_{min} = cos(\theta/2)$. A minimum damping ratio of 6.5% was chosen for both modes which corresponds to an inner angle of 3.0115 radians. The design achieves this specification for both the inter-area modes.

2) Weighting Filter Selection: The weighting filters W_1, W_2, and W_3 in Fig 6 are selected in light of the following requirements:

• **Selection of** W_1: The disturbance d as in Fig 5 is a low frequency signal and is hence penalized with a low-pass filter with the bandwidth equal to the disturbance signal d. Iteratively, W_{1_init} was best found as (9), where $K_1 = 0.05$. In order to scale it to the plant gain, a 3-stage cascade is used to obtain W_1, resulting in a 6^{th} order filter.

$$W_{1\_init}(s) = K_1 \frac{0.25}{s^2 + s + 0.25} \tag{9}$$

The added advantage of the cascade was the steepness of the low pass filter, which proved to be very effective for the disturbance attenuation at the low frequencies, and to achieve improvement in damping for the required modes. W_1 dominates in the frequency range of $(0 - 8.5$ rad/s). It should be noted that all the modes of interest are within this frequency range.

• **Selection of** W_2: The filter W_2 is selected to be a highpass filter with crossover frequency approximately equal to the closed loop bandwidth of the system. This improves control effort minimization at higher frequencies. The cut-off frequency for the high-pass filter was set to 150 rad/s to limit the magnitude of the closed loop poles of the controller. W_2 was also obtained after cascading the high-pass filter $W_{2_{init}}$ (10) in series resulting in a 6^{th} order high-pass filter, where $K_2 = 0.01$. In order to ensure that the weight W_1 dominated at the low frequencies for successful disturbance attenuation, W_2 was designed to attain a low frequency gain of -572 dB.

$$W_{2\_init}(s) = K_2 \frac{s^2}{s^2 + 120s + 3600} \tag{10}$$

• **Selection of** W_3: W_3 is weighted for the disturbance plant input matrix. It is selected as $W_3 = \alpha I$, with α designed for disturbance rejection by scaling the input of the disturbance plant as close as possible to the nominal plant. After an iterative process, $\alpha = (50 \times 10^{-6})$ is obtained to satisfy these criteria.

3) Damping Controller Design: A self-explanatory flowchart is shown in Fig. 9, which summarizes the damping controller design methodology. The original plant and the disturbance plant are reduced to a 20^{th} order equivalent by Schur Balanced Truncation [15], see Fig. 10.

The reduced plants capture the targeted inter-area modes of 0.201 Hz and 0.475 Hz. As shown in Fig. 9, the objectives of the control design is simultaneous disturbance attenuation, explicitly modeled disturbance rejection, and control effort minimization. This resulted in a 56^{th} order controller, which was reduced to 28^{th} order - the singular value plots are shown in Fig.11(a). The designed controller modulates the real power reference of the positive and negative poles of converter stations #1 and #3. The control design was performed using the Robust Control Toolbox in Matlab [22]. Table I highlights the closed-loop poles of the system with the reduced controller, which shows that a settling time of less than $15.0s$ is achieved for the targeted modes without compromising the well-damped modes.

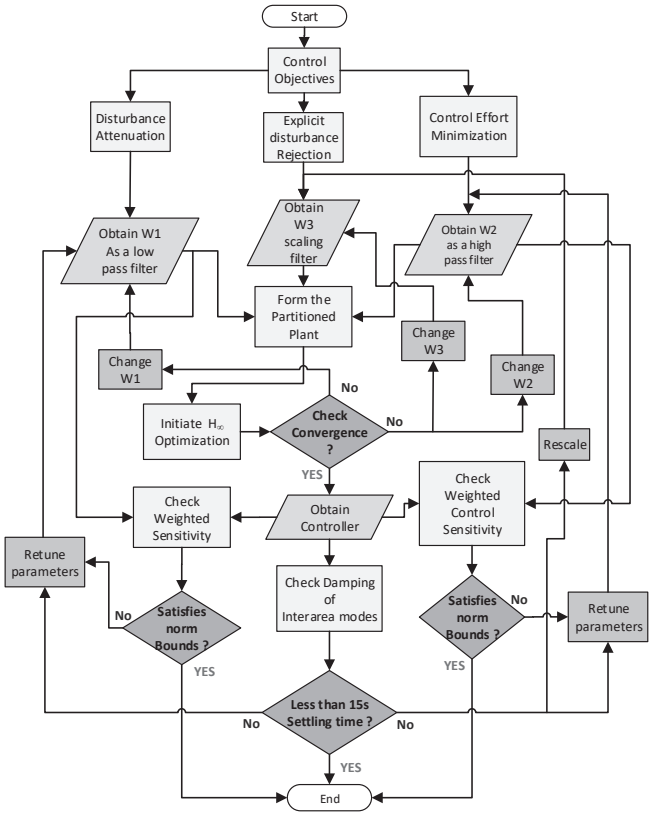

Fig. 9. Flowchart describing damping controller synthesis.

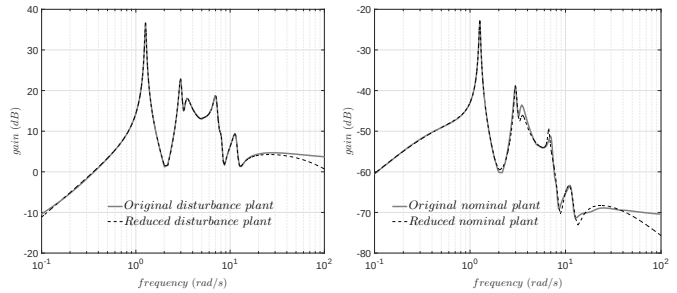

Fig. 10. Maximum singular value plot of the disturbance plant $G_d(s)$ and no

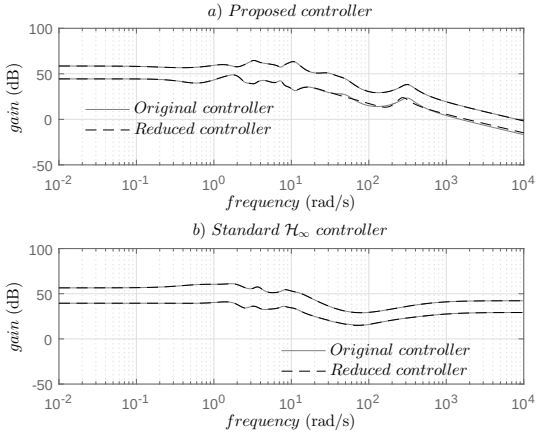

Fig. 11. Frequency response of the synthesized damping controllers: a) proposed controller, b) standard $\mathcal{H}_\infty$ controller.

D. Comparison of Performance with Standard $\mathcal{H}_\infty$ Design

A comparison study with the standard $\mathcal{H}_\infty$ design was performed to present the effectiveness of the proposed control scheme. The standard $\mathcal{H}_\infty$ design philosophy is kept the same as in [12]. The same reduced-order nominal plant was used for the control design. In order to maintain uniformity in design, the same weights (9), (10) were chosen, and cascading was performed in a similar fashion as in case of the explicit disturbance rejection design. This resulted in a 56^{th} order controller, which was reduced to 28^{th} order - the singular value plots are shown in Fig.11(b).

TABLE IV
DAMPING RATIOS, FREQUENCIES AND SETTLING TIMES OF THE INTER-AREA MODES IN TEST SYSTEM WITH STANDARD $\mathcal{H}_\infty$ CONTROL

Design Criterion, $\zeta_{min} = 15\%$						
Mode no.	OPEN-LOOP			CLOSED-LOOP		
	ζ	f, Hz	T, s	ζ	f, Hz	T, s
1.	**0.015**	0.201	204.20	**0.214**	0.192	15.17
2.	**0.033**	0.475	40.25	**0.070**	0.501	18.09
3.	0.053	0.792	15.25	0.061	0.795	13.09

Table IV shows the closed loop poles with the standard $\mathcal{H}_\infty$ design. This is the best possible closed-loop damping performance we could achieve, albeit with $\zeta_{min} = 15\%$ as design criterion, as opposed to $\zeta_{min} = 6.5\%$ used for the proposed method. Attempt to increase closed-loop damping by further increasing ζ_{min} lead to non-convergence. It can be seen in Table IV that the closed-loop damping is slightly inferior compared to the explicit disturbance rejection design, in Table I.

Figure 12 shows the comparison of control effort between the standard $\mathcal{H}_\infty$ design and the proposed design when a pulse disturbance is applied at the input of the closed-loop full-order linearized plant. The proposed controller produces slightly better damping performance at significantly lesser control effort.

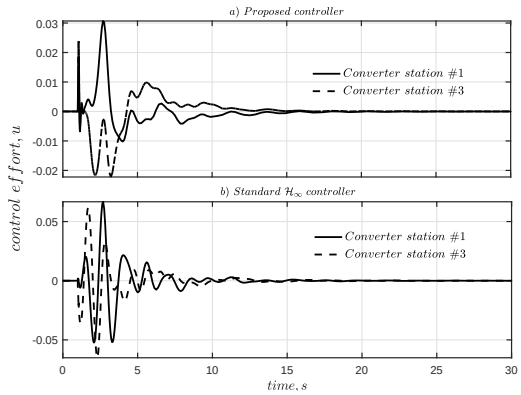

Fig. 12. Comparison of control effort between a) proposed controller and b) standard $\mathcal{H}_\infty$ controller when a pulse disturbance is applied at the input of the closed-loop full-order linearized plant.

E. Measures of Robustness

Robustness in the design can be observed from the infinity norm of the weighted sensitivity and the control times sensitivity, according to the Small Gain Theorem and the Bounded Real Lemma [15], [16]. Both the weighted functions in our proposed design satisfy the robustness criteria: $\|W_1 S\|_\infty = 1.2523 \times 10^{-4}$, $\|W_2 K S\|_\infty = 7.3755 \times 10^{-5}$. They also satisfy the robustness criterion with the standard

$\mathcal{H}_\infty$ design:

$\|W_1 S\|_\infty = 1.2518 \times 10^{-4},\ \|W_2 KS\|_\infty = 1.2889 \times 10^{-4}$.

Another measure of robustness is the smallest unstructured inverse input multiplicative perturbation at the sensitivity function that can destabilize the system. This parameter can be evaluated by placing a bound on the largest singular value of the sensitivity [23]. If we assume the perturbation as δ_0, then robust stability requires $\bar{\sigma}\left[(I-L)^{-1}\right] < \frac{1}{\delta_0}$, where $L = KG$ is the open loop gain at the plant input channels. The singular values of the input plant sensitivity are plotted in Fig. 13, which correspond to the smallest unstructured inverse input multiplicative perturbation.

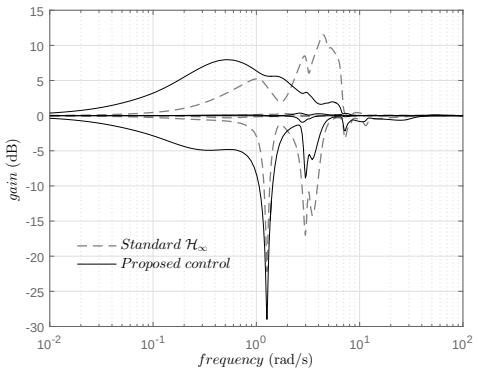

Fig. 13. Input plant sensitivity subject to the designed controllers

From Table V, it can be seen that δ_0 for the proposed controller is almost twice of that of the standard $\mathcal{H}_\infty$ controller. This indicates that the proposed control has a greater bound for the disturbance input, i.e, any perturbation in the input channels of the plant will have to be almost double the amount as compared to the standard $\mathcal{H}_\infty$ design to destabilize the system. This ensures that the disturbance attenuation property of the proposed control design is superior, which makes it more robust to disturbance input than that of the existing method.

The phase and gain margins at the input channels [23] are calculated using (11) and shown in Table V. The gain and phase margins at the input channels are comparitively better for the proposed control.

$$GM = \left[\frac{1}{1+\delta_0}, \frac{1}{1-\delta_0}\right], \quad PM = \pm\cos^{-1}[1-\frac{\delta_0^2}{2}] \tag{11}$$

TABLE V
INPUT PLANT SENSITIVITY

Control used	$\bar{\sigma}\,(I-L)^{-1}$	δ_0	GM	PM
Proposed	7.96dB	0.4	[1.67,0.714]	$\pm 23.04^\circ$
Standard $\mathcal{H}_\infty$	11.5dB	0.26	[1.32,0.79]	$\pm 15.27^\circ$

Remark: For an MTDC grid connecting offshore wind farms to onshore AC system, a combination of onshore converter stations and offshore wind farms can be used as actuators. The real power reference of the offshore wind farms can be modulated using remote PMU signals from the onshore AC grid.

V. SIMULATION RESULTS

To demonstrate robustness of the proposed control scheme, simulations were carried out for multiple contingencies, which trigger the inter-area modes. Unlike earlier works, which considered only AC-side faults, we illustrate performance following major AC as well as DC-side disturbances. From now on, we will use the legend "Explicitly modelled DR" to represent the proposed explicitly modeled disturbance rejection controller response in the plots.

A. Major Tie-Line Outages

We have considered outages of one of the tie-lines in each of the double-circuit lines connecting buses $(18-42)$, $(18-49)$, $(27-53)$ and $(40-41)$, see Fig. 8, following a 3-phase, 5-cycle fault. The faults were simulated near bus 18, 49, 27, and 40, respectively. Notably, these tie-lines interconnect the five areas in the meshed AC-MTDC system.

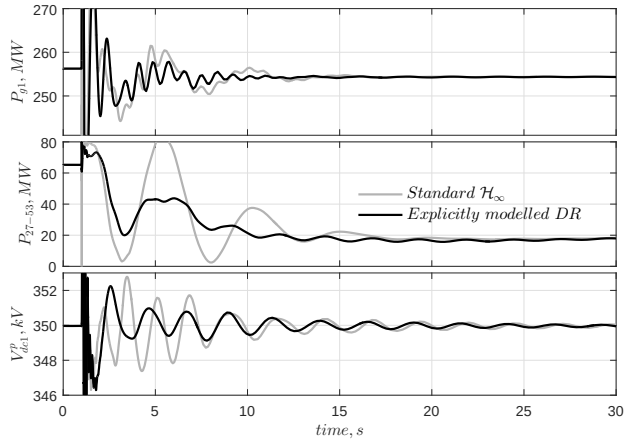

Fig. 14. Dynamic performance of the system following a 3-phase fault near bus 18 cleared after 5-cycles by the outage of one of the double-circuit lines connecting buses 18 and 42, Fig. 8, at $t = 1.0s$.

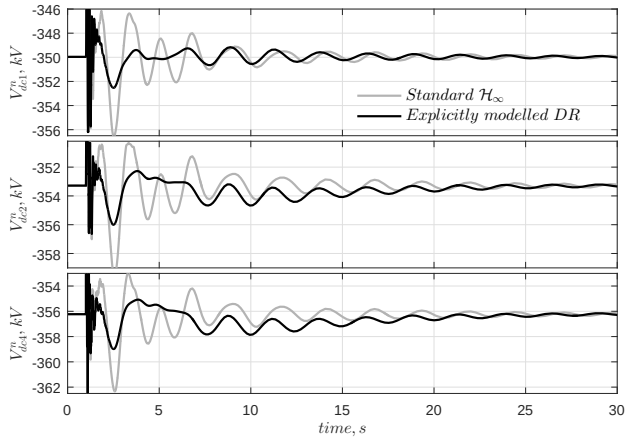

Fig. 15. DC voltage of the converter poles following a 3-phase fault near bus 18 cleared after 5-cycles by the outage of one of the double-circuit lines connecting buses 18 and 42, Fig. 8, at $t = 1.0s$.

Figures 14, 16, 18, and 19 show effective damping for outage of lines $(18-42)$,$(18-49)$, $(27-53)$ and $(40-41)$, respectively. It can be seen from Figs 14, 16, 18, and 19 that the proposed method produces similar damping performance compared to the standard $\mathcal{H}_\infty$ control, in case of major tie-line outages in the grid. This is expected since both approaches are robust control design methods. The DC voltages of the converter stations' negative and positive poles are plotted in Figs 15, 17, and 20 in the event of outage of the lines $(18-42)$,

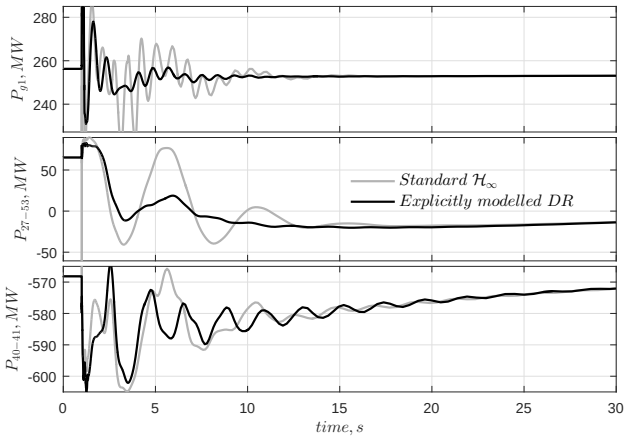

Fig. 16. Dynamic performance of the system following a 3-phase fault near bus 49 cleared after 5-cycles by the outage of one of the double-circuit lines connecting buses 18 and 49, Fig. 8, at $t = 1.0s$.

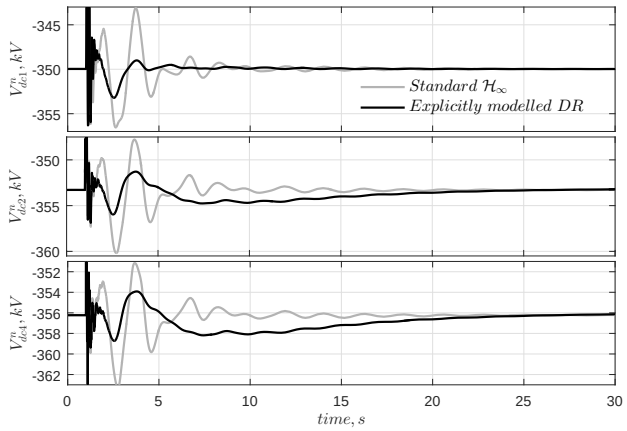

Fig. 17. DC voltage of the converter poles following a 3-phase fault near bus 49 cleared after 5-cycles by the outage of one of the double-circuit lines connecting buses 18 and 49, Fig. 8, at $t = 1.0s$.

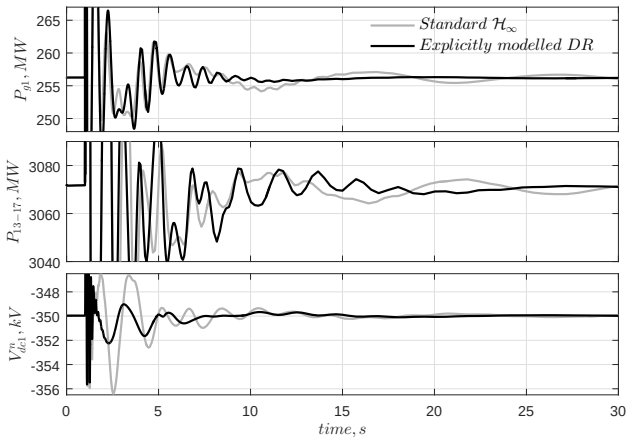

Fig. 18. Dynamic performance of the system following a 3-phase fault near bus 27 cleared after 5-cycles by the outage of one of the double-circuit lines connecting buses 27 and 53, Fig. 8, at $t = 1.0s$.

$(18-49)$ and $(40-41)$, respectively. It can be observed that the DC voltage excursions in the converter station poles during these events are lower for the proposed control design. This is a consequence of a significantly less control effort required to damp the oscillatory modes in case of the proposed approach.

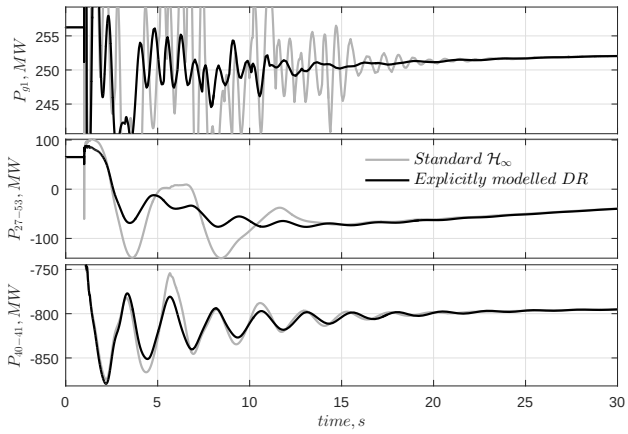

Fig. 19. Dynamic performance of the system following a 3-phase fault near bus 40 cleared after 5-cycles by the outage of one of the double-circuit lines connecting buses 40 and 41, Fig. 8, at $t = 1.0s$.

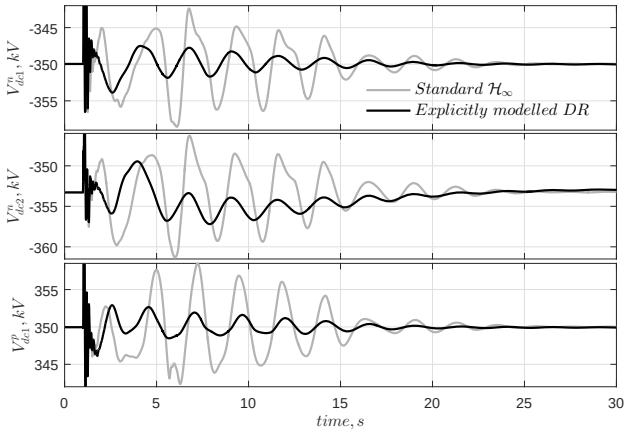

Fig. 20. DC voltage of the converter poles following a 3-phase fault near bus 40 cleared after 5-cycles by the outage of one of the double-circuit lines connecting buses 40 and 41, Fig. 8, at $t = 1.0s$.

B. Converter Station Outage

1) Negative pole outage at converter station #2

Figures 21 and 22 show the dynamic performance of the system following the outage of the negative pole of converter station #2. It can be seen that – (a) At $t = 1.0s$ the real power output of converter #2 negative pole becomes zero; (b) The explicitly modelled disturbance rejection $\mathcal{H}_\infty$ damping controller is able to damp the oscillatory modes better than the standard $\mathcal{H}_\infty$ controller; (c) Major line power flows have been shown in Fig. 21 whereas Fig. 22 shows DC voltages of the negative and positive poles of the converter stations.

2) Actuator outage: Negative pole outage at converter station #3

Converter station #3 was used as an actuator in the control design. The outage of one pole of converter #3 may have serious consequences, if it is not considered in the design phase of the controller. Figure 23 shows that despite the outage of the actuator, the proposed damping controller demonstrates strong disturbance rejection properties. The actuator #3 outage can been seen from the first subplot in Fig. 23.

It can be observed that the proposed controller produces better damping performance in the event of actuator outage-a

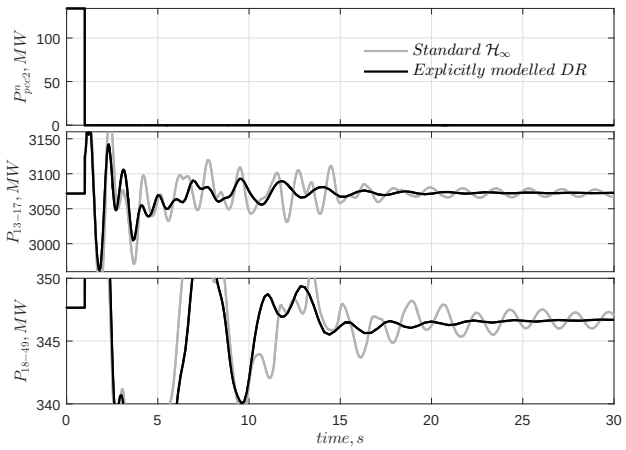

Fig. 21. Dynamic performance of the system following the outage of the negative pole of converter station #2 at $t = 1.0s$.

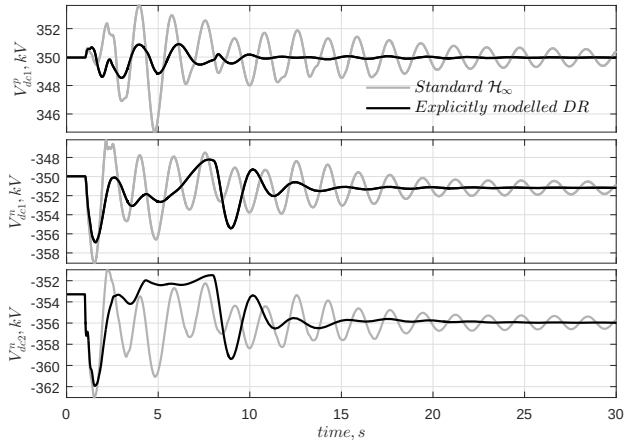

Fig. 22. DC voltage of the converter poles following the outage of the negative pole of converter station #2 at $t = 1.0s$.

major DC-side contingency scenario. Figure 24 shows the DC voltage of converter station #1's positive and negative pole in the first two subplots, and the power modulation in the positive pole of converter #4 in the last subplot.

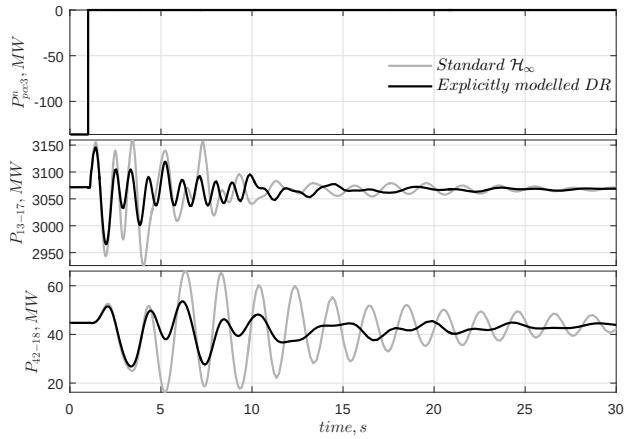

Fig. 23. Dynamic performance of the system following the outage of the negative pole of converter station #3 at $t = 1.0s$.

The damping performance of the standard $\mathcal{H}_\infty$ controller is comparatively inferior to the proposed controller in case of major DC-side outages, see Figs 21, 23. Moreover, the

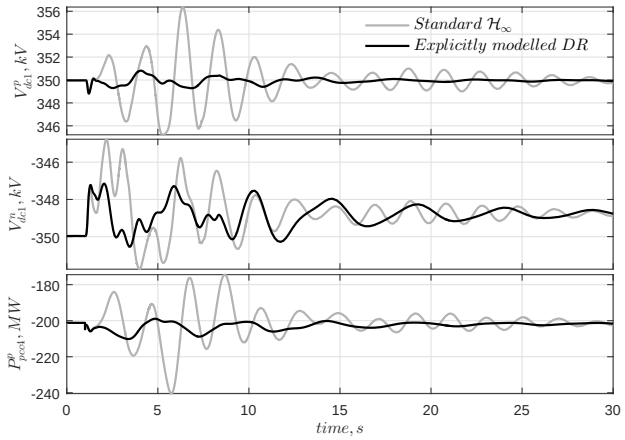

Fig. 24. Dynamic performance of the system following the outage of the negative pole of converter station #3 at $t = 1.0s$.

DC voltage profiles in the converter station poles in Figs 22 and 24 show huge excursions with the standard $\mathcal{H}_\infty$ control due to higher control effort requirement. On the contrary, the proposed controller produces lesser fluctuations in the DC voltages. These results confirm the benefits of the novel concept of explicitly modeling the disturbances for controller design, as this approach produces better damping performance with lesser control effort for AC as well as DC-side outages.

C. Feedback Signal Loss

Figure 25 shows the dynamic performance of the damping controller with the loss of the feedback signal P_{13-17}, following the outage of one of the double-circuit lines connecting buses 18 and 49 at $t = 1.0s$. A similar damping performance can be observed for both the design approaches.

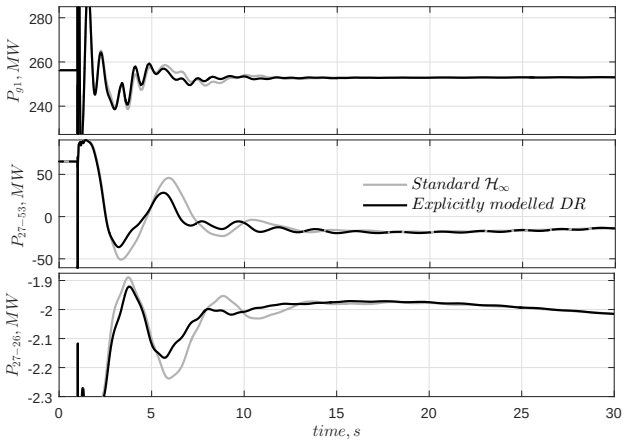

Fig. 25. Dynamic performance of the system with the loss of feedback signal P_{13-17}, following the outage of one of the double-circuit lines connecting buses 18 and 49 at $t = 1.0s$.

D. Communication Latency

To demonstrate the robustness of the controller performance following (a) converter #2 negative pole outage and (b) outage of one of the double circuit lines connecting buses 18 and 42 are studied in presence of a 100 ms latency in the feedback signals. The effectiveness of the controller in presence of

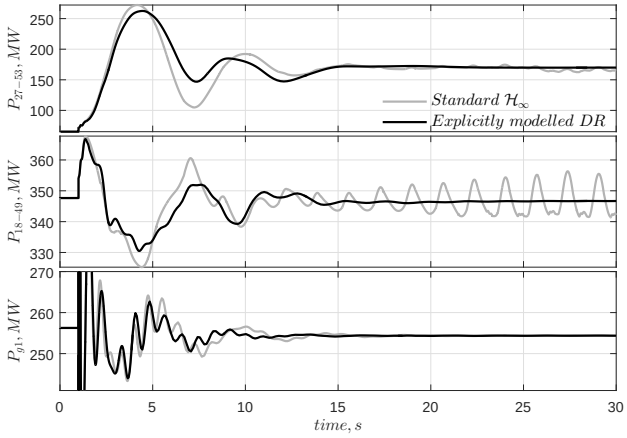

Fig. 26. Dynamic performance of the system with 100 ms latency following the outage of a) first two subplots - the negative pole of converter station #2 at $t = 1.0s$. b) last subplot - one of the double-circuit lines connecting buses 18 and 42 at $t = 1.0s$.

latency can be seen in Fig. 26 following the converter and the line outage scenarios.

It is interesting to note that for the AC line outage, see the last subplot in Fig. 26, the standard $\mathcal{H}_\infty$ controller produces a similar performance as the proposed controller. However, in case of the DC outage, shown in the first two subplots in Fig. 26, the standard $\mathcal{H}_\infty$ controller fails to maintain stability. This further substantiates the need for explicitly modeling disturbances in the control formulation to take into account such events that can cause the standard $\mathcal{H}_\infty$ control technique to fail.

VI. Conclusion

This paper presents a new approach for robust power oscillation damping in MTDC grids connected to AC systems. The novelty consists in modifying the $\mathcal{H}_\infty$ control design approach where disturbances can be viewed and accounted explicitly in terms of MTDC current injections. This problem is solved by an updated mixed sensitivity formulation in the Linear Matrix Inequality (LMI) framework. The resulting MIMO controller uses wide-area signals to stabilize poorly-damped inter-area modes without compromising well-damped modes. Control performance and robustness are assessed with dynamic simulations on a 16-machine 5-area system connected to a 4-terminal asymmetric bipolar MTDC grid. The unique aspect of the proposed controller is its robustness to severe disturbances on the AC as well as DC side - including loss of actuators. In addition, the proposed controller is able to maintain acceptable performance in the wake of communication latencies and partial signal loss. The proposed design approach shows superior performance compared to a standard $\mathcal{H}_\infty$ design.

References

[1] Cole, S.; Beerten, J.; Belmans, R., "Generalized Dynamic VSC MTDC Model for Power System Stability Studies," *IEEE Transactions on Power Systems* , vol.25, no.3, pp.1655-1662, Aug. 2010.

[2] Chaudhuri, N.R.; Majumder, R.; Chaudhuri, B.; Jiuping Pan, "Stability Analysis of VSC MTDC Grids Connected to Multimachine AC Systems," *IEEE Transactions on Power Delivery* , vol.26, no.4, pp.2774-2784, Oct. 2011.

[3] Chaudhuri, N.R.; Chaudhuri, B., "Adaptive Droop Control for Effective Power Sharing in Multi-Terminal DC (MTDC) Grids," *IEEE Transactions on Power Systems* , vol.28, no.1, pp.21-29, Feb. 2013.

[4] Prieto-Araujo, E.; Bianchi, F.D.; Junyent-Ferre, A.; Gomis-Bellmunt, O., "Methodology for Droop Control Dynamic Analysis of Multiterminal VSC-HVDC Grids for Offshore Wind Farms," *IEEE Transactions on Power Delivery* , vol.26, no.4, pp.2476-2485, Oct. 2011.

[5] Eriksson, R.; Beerten, J.; Ghandhari, M.; Belmans, R., "Optimizing DC Voltage Droop Settings for AC/DC System Interactions," *IEEE Transactions on Power Delivery* , vol.29, no.1, pp.362-369, Feb. 2014.

[6] Preece, R.; Milanovic, J.V., "Tuning of a Damping Controller for Multiterminal VSC-HVDC Grids Using the Probabilistic Collocation Method," *IEEE Transactions on Power Delivery* , vol.29, no.1, pp.318-326, Feb. 2014.

[7] Eriksson, R., "A New Control Structure for Multi-Terminal dc Grids to Damp Inter-Area Oscillations," in Early Access, *IEEE Transactions on Power Delivery*, 2014.

[8] L. Harnefors, N. Johansson, L. Zhang and B. Berggren, "Interarea Oscillation Damping Using Active-Power Modulation of Multiterminal HVDC Transmissions," in *IEEE Transactions on Power Systems*, vol. 29, no. 5, pp. 2529-2538, Sept. 2014.

[9] A. McDonald and C.Clack, "Low cost and low carbon emission wind and solar energy systems are feasible for large geographic domains," in *Sustainable Energy and Atmospheric Sciences Seminar*, NOAA, NREL, and CU-Boulder RASEI, May 2014.

[10] Y. Li and J. D. McCalley, "Design of a High Capacity Inter-Regional Transmission Overlay for the U.S.," in *IEEE Transactions on Power Systems*, vol. 30, no. 1, pp. 513-521, Jan. 2015.

[11] P. Agnihotri; A. Kulkarni; A. Gole; B. Archer; T. Weekes, "A Robust Wide-Area Measurement Based Damping Controller for Networks with Embedded Multi-Terminal and Multi-Infeed HVDC Links," in *IEEE Transactions on Power Systems* , vol.PP, no.99, pp.1-1

[12] A. Banerjee and N. R. Chaudhuri, "Robust Damping of Inter-Area Oscillations in AC-MTDC grids using H_∞ Mixed-sensitivity approach," in proceedings of *Power and Energy Society General Meeting (PESGM)*, 2016.

[13] Chaudhuri, N.R.; Chaudhuri, B.; Majumder, R.;, Yazdani, A., *Multi-terminal Direct-Current Grids: Modeling, Anlysis, and Control.* Wiley-IEEE Press, 2014.

[14] Pal, B. and Chaudhuri, B., *Robust Control in Power Systems.* Springer, 2005.

[15] S. Skogestad and I. Postlethwaite, *Multivariable Feedback Control.* New York: Wiley, 2001.

[16] Gahinet, P. and Apkarian, P. (1994), "A linear matrix inequality approach to H_∞ control". *Int. J. Robust Nonlinear Control* , 4: 421448.

[17] Scherer, C.; Gahinet, P.; Chilali, M., "Multiobjective output-feedback control via LMI optimization," *IEEE Transactions on Automatic Control* , vol.42, no.7, pp.896-911, Jul 1997.

[18] Chilali, M.; Gahinet, P., "H_∞ design with pole placement constraints: an LMI approach," *IEEE Transactions on Automatic Control* , vol.41, no.3, pp.358-367, Mar 1996.

[19] Chaudhuri, B.; Pal, B.C.; Zolotas, A.C.; Jaimoukha, I.M.; Green, T.C., "Mixed-sensitivity approach to H_∞ control of power system oscillations employing multiple FACTS devices," *IEEE Transactions on Power Systems*, vol.18, no.3, pp.1149-1156, Aug. 2003.

[20] Chaudhuri, B.; Pal, B.C., "Robust damping of multiple swing modes employing global stabilizing signals with a TCSC," *IEEE Transactions on Power Systems*, vol.19, no.1, pp.499-506, Feb. 2004.

[21] Ray, S. and Chaudhuri, B. and Majumder, R., "Appropriate signal selection for damping multi-modal oscillations using low order controllers," in 2008 IEEE Power and Energy Society General Meeting - Conversion and Delivery of Electrical Energy in the 21st Century, July 2008.

[22] *Matlab Users Guide*, The Math Works Inc., USA, 2015.

[23] N. Lehtomaki, D. Castanon, B. Levy, G. Stein, N. Sandell and M. Athans, "Robustness and modeling error characterization," in *IEEE Transactions on Automatic Control*, vol. 29, no. 3, pp. 212-220, Mar 1984.

[24] Cao, Y. *Control Structure Selection for Chemical Processes Using Input-Output Controllability Analysis*, PhD thesis, University of Exeter, 1995.

Abhishek Banerjee (S'15) received his B.Tech degree from the West Bengal University of Technology, West Bengal, India in 2014. He is currently pursuing his Ph.D. degree in the Department of Electrical and Computer Engineering at North Dakota State University, Fargo, ND, USA.
His research interests include control theory, application of advanced control to power systems, wide-area monitoring and control, wide-area resilient protection, power system dynamics and control, MTDC, and renewable energy.

Nilanjan Ray Chaudhuri (S'08-M'09-SM'16) received his Ph.D. degree from Imperial College London, London, UK in 2011 in Power Systems. From 2005-2007, he worked in General Electric (GE) John F. Welch Technology Center. He came back to GE and worked in GE Global Research Center, NY, USA as a Lead Engineer during 2011-2014. Presently, he is an Assistant Professor with the School of Electrical Engineering and Computer Science at Penn State, University Park, PA. He was an Assistant Professor with North Dakota State University, Fargo, ND, USA during 2014-2016. He is a member of the *IEEE* and *IEEE PES*. Dr. Ray Chaudhuri is the lead author of the book *Multi-terminal Direct Current Grids: Modeling, Analysis, and Control* (Wiley/IEEE Press, 2014), and an Associate Editor of the IEEE TRANSACTIONS ON POWER DELIVERY. Dr. Ray Chaudhuri is the recipient of the National Science Foundation Early Faculty CAREER Award in 2016.

Rajesh G. Kavasseri (M02) received the B.E. degree from Visvesvaraya Regional College of Engineering, Nagpur, India, in 1995, the M.S. degree from the Indian Institute of Science, Bangalore, India, in 1998, and the Ph.D. degree from Washington State University, Pullman, WA, USA, in 2002, all in electrical engineering. His research interests focus on power systems analysis and computing. Since 2002, he has been with the Department of Electrical and Computer Engineering,North Dakota State University, Fargo, ND, USA, where he is currently an Associate Professor.